

7

Results

In this chapter, we present several results on flows with suspended and floating particles, obtained using the fictitious domain formulation and Lagrange multipliers that we propose in this thesis. We validate our formulation and implementation in Sections 7.1, 7.2 and 7.4 by comparing the results in different test problems that simulate the fluid–particle iteration for one or more particles in a closed box. The agreement with previous and theoretical results was excellent. We also performed a parametric study of our formulation in more complex and non–standard particulate flow (see Section 7.3) and floating particles (see Section 7.5) test problems.

For all results presented on this chapter, we included one figure (that is the composition of images) illustrating the test case dynamics. The first image in each figure (except in the last three tests) is the overlap of the particle’s position obtained from some chosen key frames of the simulation. The other images are the full representation of each key frame and include also the fluid’s velocity field representation. The fluid’s velocity is colored according with its magnitude. In all images, the cross marks inside each particle helps us to visualize the angular orientation change of the particles during the simulation.

7.1

Single particle sedimentation

The first test case presented is the sedimentation of one particle in a closed box. The results are shown in Figure 7.1. The complete set of parameters is the following: the domain Ω is a closed box parametrized by $[-0.286, 0.286] \times [-1.0, 1.0]$, discretized by a mesh of 504 squared elements with \mathbb{P}_4 – \mathbb{P}_2 finite elements basis functions. The fluid phase Ω_f is a Newtonian incompressible fluid with density $\rho_f = 1.0$. The fluid’s viscosity is $\mu_f = 0.01$. A single particle with radius $R_p = 0.0714$ and density $\rho_p = 1.5$ is embedded on the fluid. The particle is initially at rest and at position $\vec{X}_p = (0, 0.869)$. The simulation’s time step is $\delta t = 0.01$ deciseconds and the total simulated time is 10 deciseconds. Finally, following the work of Diaz-Goano et al (2003)(9), we set the Lagrange multiplier parameter α to be 150.

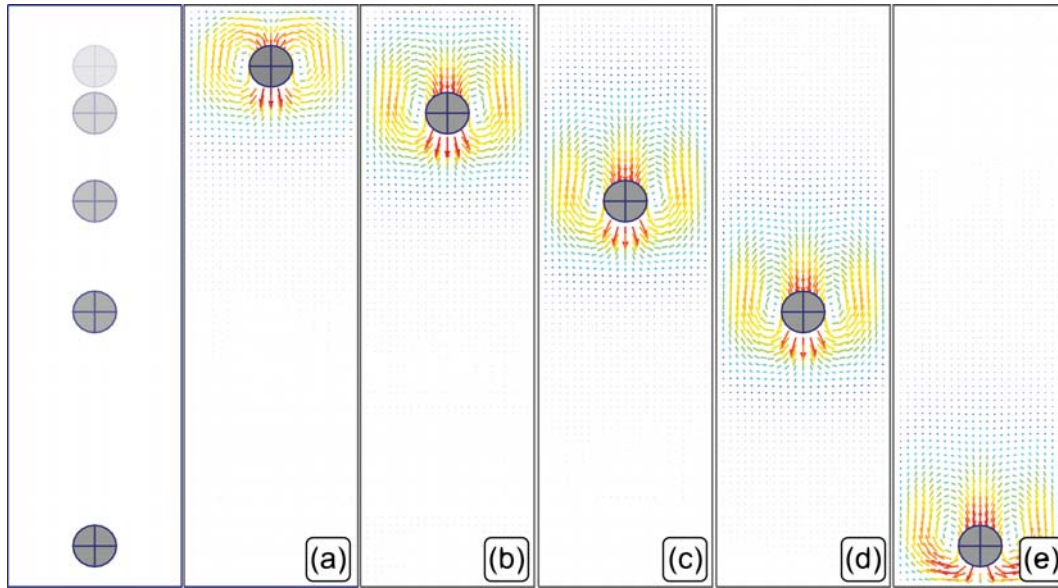


Figure 7.1: Single particle sedimentation: a particle of density 1.5 embedded on a incompressible fluid of viscosity 0.01 and density 1.0 falling under the gravity force. Images (a)–(e) show the particle’s position and the fluid’s velocity at 0.6, 1.3, 2.5, 4 and 5.5 *ds* of simulated time.

Figure 7.2 shows the evolution of the particle’s velocity for different particle’s densities, which varies from 1.5 to 1.8. The particle accelerates until it reaches a terminal velocity. The magnitude U_t of the terminal velocity of a cylinder falling in a box in the limiting case of $\text{Re} \rightarrow 0$ can be evaluated based on the drag force acting on the cylinder. The magnitude of the drag force is obtained through an asymptotic solution of the Stokes’ problem (31):

$$F_d = \frac{4\pi\mu_f}{\Delta} \frac{3}{2} U_t, \quad (7-1)$$

where,

$$\Delta = U_0 - (1 + \sum_i W_i \Gamma^i) \ln(\Gamma) + \sum_i V_i \Gamma^i.$$

The ratio of the cylinder radius to the box half-width is denoted by $\Gamma = R_p/w$, $U_0 = -0.915689$ and the even-numbered dimensionless coefficients W_i and V_i are shown in Table 7.1:

W_2	0.5	V_2	1.26654
W_4	0.054648	V_4	-0.91804
W_6	-0.264629	V_6	1.87710
W_8	0.792986	V_8	-4.66549

Table 7.1: Dimensionless coefficients for the computation of the drag force using the asymptotic solution of the Stokes’ problem.

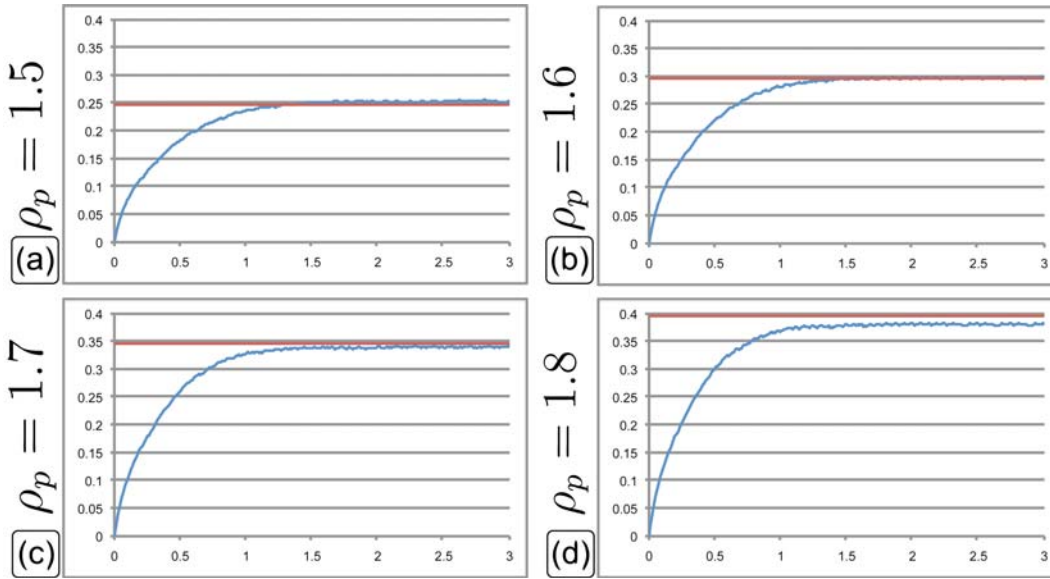


Figure 7.2: Evolution of the particle's velocity in the sedimentation case using different densities for the particle: In Figure (a) the particle's density is 1.5, in (b) $\rho_p = 1.6$, in (c) $\rho_p = 1.7$ and finally in (d) $\rho_p = 1.8$.

If we suppose that the drag force \vec{F}_d is equal the relative weight of the particle when it reaches the terminal velocity, that is $F_d = P - E$ with, P and E being the particle's weight and the buoyancy force respectively, we get an theoretical expression for the magnitude U_t of the terminal velocity:

$$U_t = \frac{2(\rho_f - \rho_p)R_p^2 g \Delta}{3 \cdot 4\pi\mu_f} \quad (7-2)$$

The red horizontal line on each graph of Figure 7.2 represents the theoretical terminal velocity obtained using the previous expression. As we can see, the agreement with the simulated terminal velocities is excellent, except for the higher particle density. The reason is that, in this case, the particle Reynolds' number, e.g. $Re \approx 10$, is not small enough for the validity of Equation 7-2.

For the flow around a falling cylindrical particle, the Reynolds number is computed using the magnitude of the terminal velocity reached by the particle, its radius and the fluid properties, more precisely its density and viscosity:

$$Re = \frac{2\rho_f U_t R_p}{\mu_f} \quad (7-3)$$

In order to evaluate the effect of the Reynolds number on the terminal velocity, we plot the dimensionless terminal velocity $\mathbf{u} = \frac{\mu_f U_t}{(\rho_f - \rho_p)R_p^2 g}$ as a function of Reynolds number, defined by Equation 7-3, in Figure 7.3. As we can observe, if the Reynolds number is above $Re \geq 10$, creeping flow approximations cannot be used.

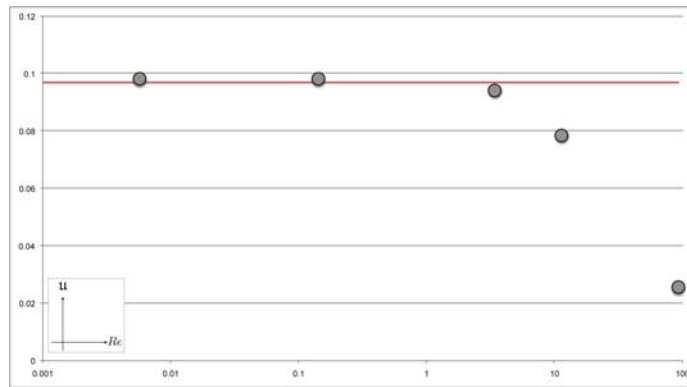


Figure 7.3: Dimensionless velocity as function of the Reynolds number: the magnitude of the velocity increases on flows with high Reynolds. The Reynolds number axis is plot using a logarithmic scale.

As shown during the derivation of the formulation, the Lagrange multipliers imposes the rigid body constraint to the fluid's velocity onto the particle's region Ω_p , avoiding viscous deformations inside each particle. Figure 7.4, shows the Lagrange multipliers and the constrained velocity field solution obtained by our code in a given frame on the single particle sedimentation test case, presented in Figure 7.1. Notice that the solution is symmetric along a vertical line passing through the center of the particle, and this behavior keeps the angular orientation unchanged during all the simulation. In this figure, the vectors of the Lagrange multipliers are normalized for better visualization, and their modulus are represented by colors that scale from blue to red. The gray circle shows the boundary of the particle's domain. It is clear that the velocity field inside the particle corresponds to a rigid body motion, which in this particular case is a constant velocity.

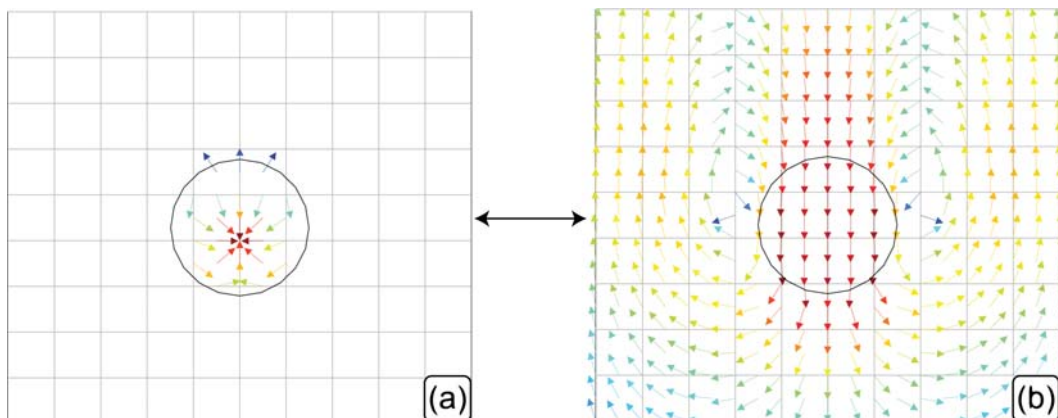


Figure 7.4: Zoom in the Lagrange multipliers effect over the velocity field in the particle sedimentation test. The Lagrange multipliers are non-zero only inside the particle region as we can see in Figure (a). It enforces the rigid body constraint inside the particle, as we observe in Figure (b).

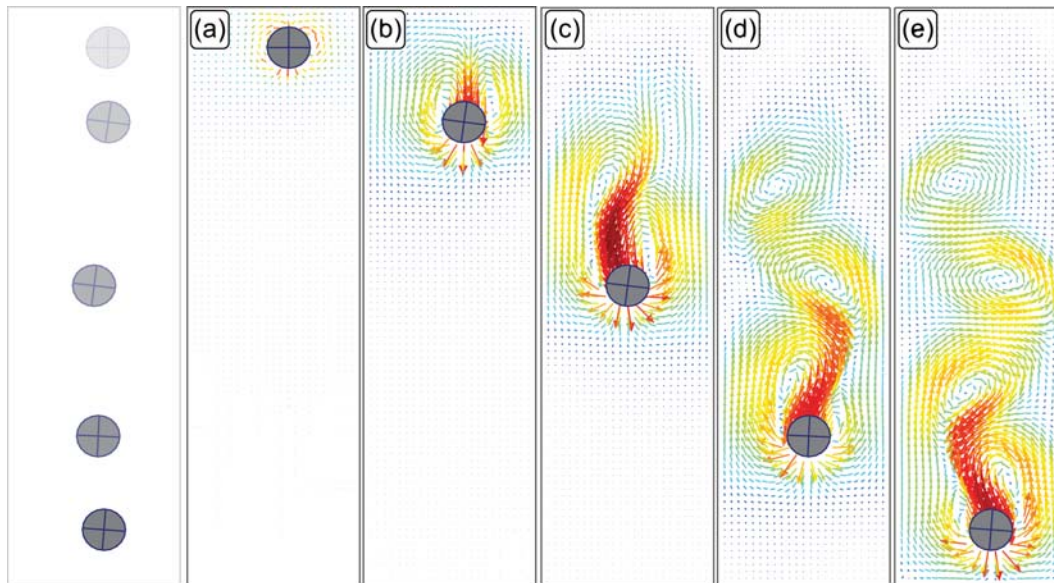


Figure 7.5: Single particle sedimentation: a particle not aligned with the vertical line that divides the domain, with density 1.5 embedded on a incompressible fluid of viscosity 0.001 and density 1.0 falling under the gravity force.

The example shown in Figure 7.5 clearly shows the coupling between the flow and the particle dynamics. The problem is the same as the one presented in Figure 7.1, except from the fact that the fluid's viscosity is now set to be $\mu_f = 0.001$ and the particle's initial position is not aligned with the vertical line that equally divides the domain, more precisely $\vec{X}_p = (0.05, 0.869)$. With the lower fluid viscosity, the particle velocity is higher and so is the Reynolds number of the flow. A periodic flow motion develops in the wake of the cylinder as the result of the von Karman vortices. The asymmetry of the flow is clear in Figure 7.5(c). In this case, the particle does not fall vertically.

7.2

Drafting, kissing and tumbling

The next test problem is the sedimentation of two cylindrical particles (see Figure 7.6), which is a benchmark for particulate flows and is known as the drafting, kissing and tumbling problem.

The complete set of parameters for the simulation is the following: the domain Ω is a closed box with dimensions $[-0.5, 0.5] \times [-1.0, 1.0]$, discretized by a mesh of 350 square elements with \mathbb{P}_4 - \mathbb{P}_2 finite elements basis functions. The fluid phase Ω_f is a Newtonian incompressible fluid with density $\rho_f = 1.0$ and viscosity $\mu_f = 0.01$. Two cylindrical particles with radius $R_{1,2} = 0.0514$ and density $\rho_{1,2} = 1.5$ are embedded on the fluid. The particles are initially at rest and at position $\vec{X}_1 = (0.015, 0.9)$ and $\vec{X}_2 = (-0.015, 0.75)$. The simulation's time step is $\delta t = 0.01$ deciseconds and the total simulated time is

10 deciseconds. Again, we set the Lagrange multiplier parameter α to be 150, following the work of Diaz-Goano et al (2003)(9).

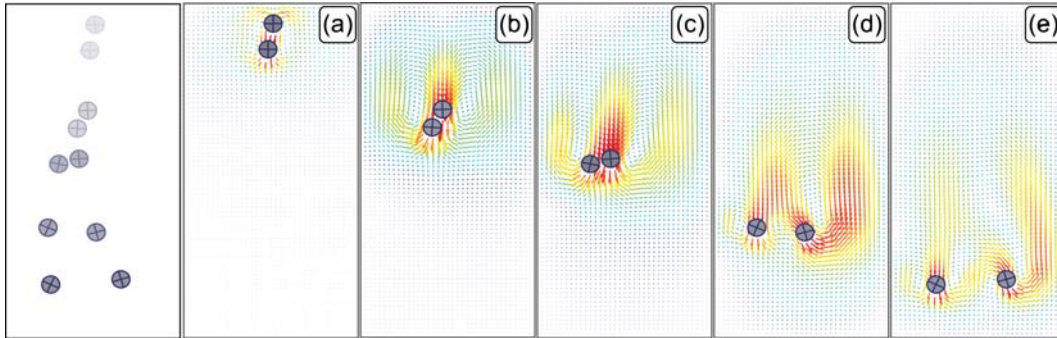


Figure 7.6: Two particles sedimentation: two particles of density 1.5 embedded in an incompressible fluid of viscosity 0.01 and density 1.0 falling under the gravity force. We can observe that the simulation reproduces the particles' interaction dynamics usually called drafting, kissing and tumbling.

Particle pair interactions are a fundamental mechanism that enter strongly into all practical applications of flows with suspended particles. The flow generated by one particle's motion contributes to the motion of another particle. The principal interactions between neighboring cylindrical particles in Newtonian liquids can be described as drafting, kissing and tumbling.

When one falling cylinder enters the wake of another, it experiences reduced drag, drafts downward toward the leading particle, and almost touches it, a phenomenon generally referred to as kissing. The two kissing particles momentarily form a single long body aligned parallel to the stream. But the parallel orientation for a falling long body is unstable and the pair of kissing particles tumbles to a side-by-side configuration. Two touching particles falling side-by-side are pushed apart until a stable separation distance between centers across the stream is established; they then fall together without further lateral migrations.

The drafting, kissing and tumbling dynamics can be easily observed on Figures 7.6 and 7.7. The blue lines on the profiles of Figure 7.7 refer to the particle initially at the higher position, and the red ones describe the profiles of the particle initially at the lower height.

Analyzing the profiles, we observe that the *drafting stage* takes place from the beginning of the simulation until approximately $2.5 ds$, since the second coordinate of the position profiles decreases until its intersection. This indicates that the particle initially at the higher position was on the wake of the lower particle that increased its velocity. The *kissing stage* begins near $2.5 ds$ and goes until $3.75 ds$ when the particles almost touch each other and change their positions (the particle initially higher becomes lower). Finally, in the *tumbling*

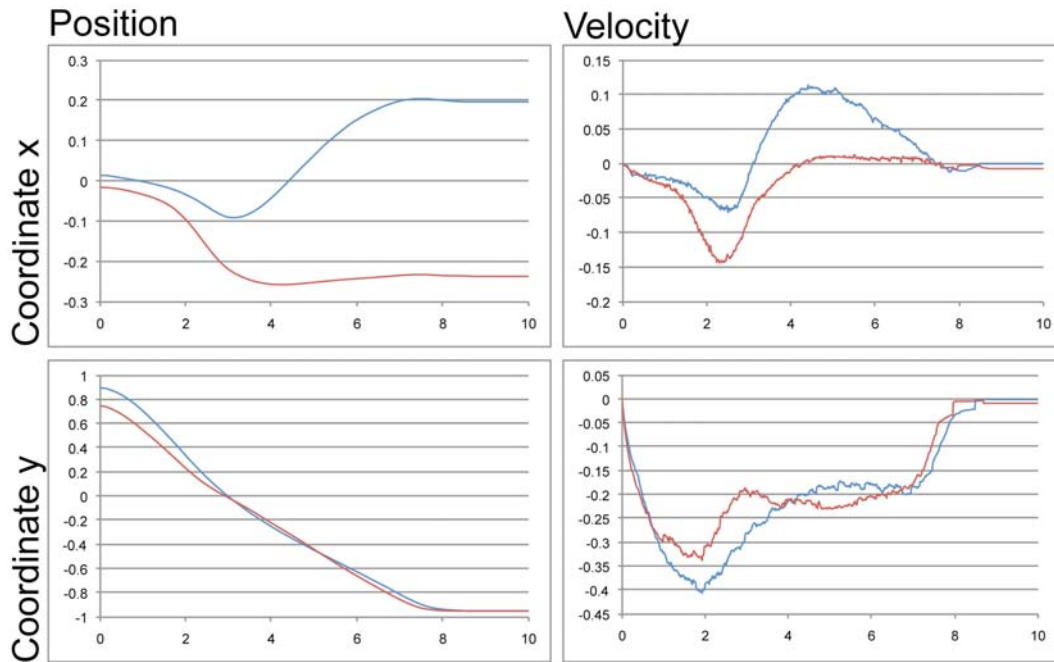


Figure 7.7: Two particles sedimentation: time history of the coordinate functions of the position and velocity solution obtained from the drafting, kissing and tumbling simulation illustrated on Figure 7.6.

stage we observe that the first velocity's coordinate function converges to zero and indicates that the particles are falling side by side. The total time in this example was 10 *ds* and the particles reach the bottom wall near to 8 *ds*.

The last example, shown in Figure 7.8, plots the comparison between the position time histories obtained using our code and the ones of the work of Wan and Turek (2007) (43). In this example the dimensions of the box were $[-1.0, 1.0] \times [-2.5, 2.5]$, the initial position of the particles were $\vec{X}_1 = (0.01, 2.0)$, $\vec{X}_2 = (0.0, 1.5)$, the fluid's properties were $\mu_f = 0.01$ and $\rho_f = 1.0$ and the particle density $\rho_p = 1.5$. As we can see the agreement of the trajectories is good, which again validates our code.

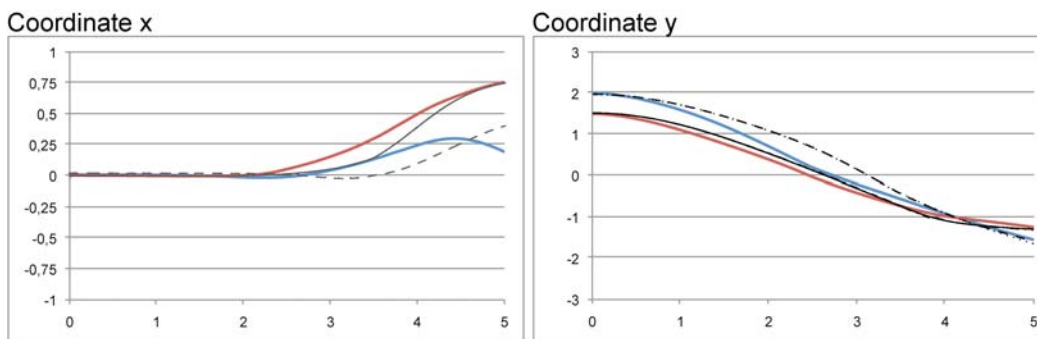


Figure 7.8: Two particles sedimentation: time history of the first (left) and second (right) coordinate functions of the position and its comparison with the results of (43), which are shown in black.

7.3

Particles dragged by the fluid

The next test problem studies the motion of cylindrical particles that are being dragged by the flow inside a lid-driven cavity. The aim of this test case is to show the capability of the method to study sediment transport.

As we said in Chapter 3, the lid-driven cavity problem has been used as a test or validation case for new codes or new solution methods because the problem geometry is simple, the boundary conditions are also easy to model and the flow is quite complex with the presence of recirculation. The standard case is a fluid contained in a square domain with Dirichlet boundary conditions on all sides, with three stationary sides and one moving side (with velocity tangent to the side). In our test case, a solid cylindrical particle is also embedded on the fluid.

The complete set of parameters for the simulations shown on Figure 7.9 is the following: the domain Ω is a closed box with dimensions $[-1.0, 1.0] \times [-0.25, 0.25]$ whose lid moves with velocity $\vec{u}_l = (1, 0)$, and is discretized by a mesh of 400 squared elements. The fluid phase Ω_f is a Newtonian

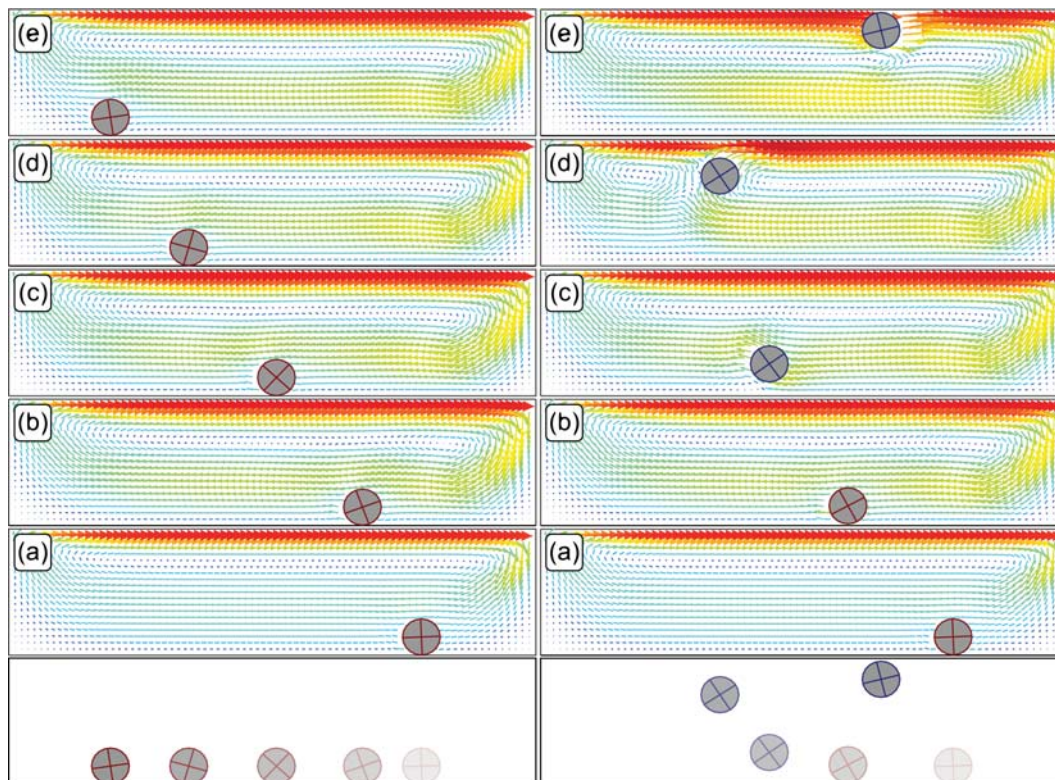


Figure 7.9: Particle dragged by the fluid: when the particle is heavier than the fluid (left column) the particle is dragged by the fluid on the bottom wall, when the particle is lighter than the fluid (right column), it moves upwards and floats in the upper side of the cavity.

incompressible fluid with density $\rho_f = 1.0$ and viscosity is $\mu_f = 0.01$. One cylindrical particle with radius $R_p = 0.0714$ is embedded on the fluid.

The particle is initially at rest at position $\vec{X}_p = (0.0, 0.177)$. The sequence shown in the left column of Figure 7.9 presents the results for particle density equal to 1.5 while the right column, the results for particle density equal to 0.5. The simulation's time step is $\delta t = 0.02$ and the total time 10 *ds*. The Lagrange multiplier parameter is $\alpha = 150$.

Observe that if the particle's density is larger than the fluid's density (see Figure 7.9 and 7.10, left) the hydrodynamic forces are not strong enough to lift the particle from the bottom wall so it is dragged towards the left until the end of the simulation. When the particle is lighter than the fluid (see Figure 7.9, right and 7.10, left), it moves upwards and it ends up floating near the up-right corner of the cavity.

Figure 7.10 shows time history of the particle's position and velocity using several scenarios. Our goal is to show the sensitivity of the results with respect to the particle's density, the lid's velocity and the cavity's width. On

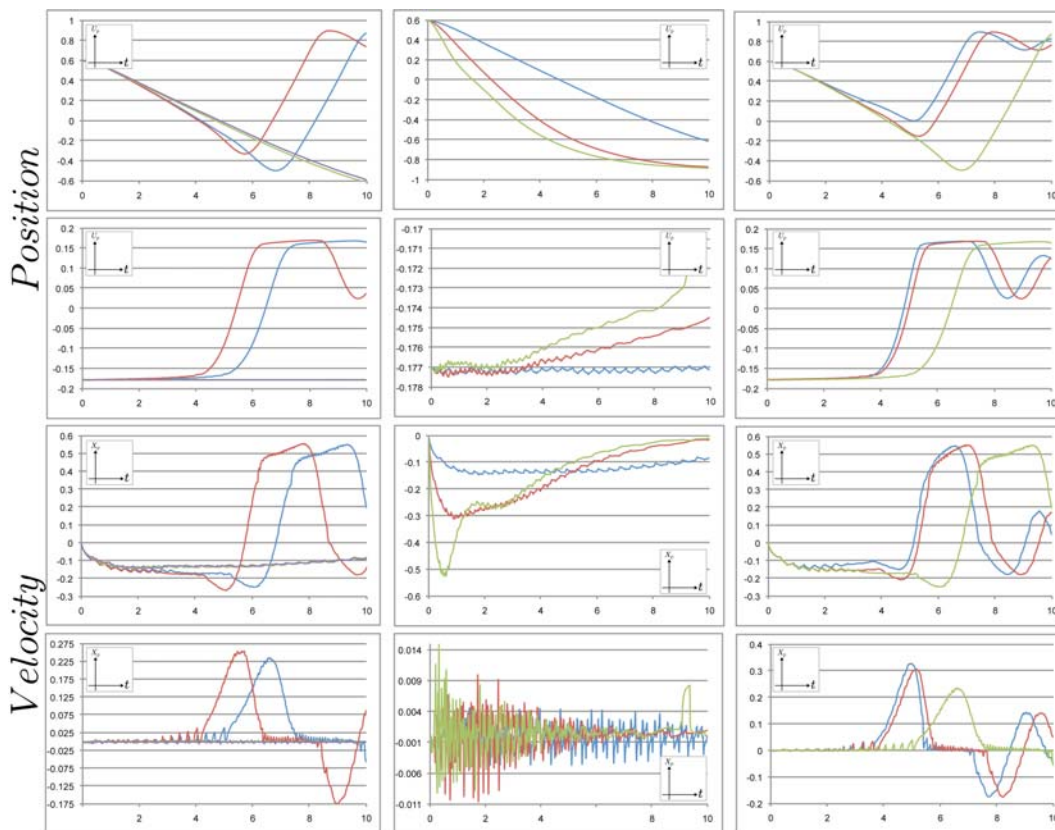


Figure 7.10: Particle dragged by the fluid: time history of the particle's position and velocity when we change its density (left column), the lid's velocity (middle column) and the cavity's width (right column). In the lid test we set the particle's density to be bigger than the fluid while in the width testes its density was smaller than the fluid.

the first column, the particle's density was 0.32 (red), 0.5 (blue), 1.0 (green) and 1.5 (purple). On the second column, the particle's density was $\rho_p = 1.0$ and the lid's velocity were $\vec{u}_l = (1.0, 0.0)$ (blue), $\vec{u}_l = (2.5, 0.0)$ (red) and $\vec{u}_l = (5.0, 0.0)$ (green). On the last column, $\rho_p = 0.2$ and the cavity's width were 1.3 (blue), 1.5 (red) and 2.0 (green). For all tests the fluid's viscosity was $\mu_f = 0.01$. The results presented in the first column show that at these conditions, the drag force is weak and particles heavier than the liquid are not suspended.

The time histories presented in Figure 7.10 (middle) show that if we increase the lid velocity, heavy particles reach bigger horizontal velocities since the velocity of the lid determines the drag force acting on the particle. The first coordinate of the particle's velocity together with the first coordinate of the particle's position show that low lid velocities produce almost zero acceleration on the particle, while high lid's velocity create big variations on the particle's acceleration. Observe that the second coordinate of the particle's position show that the particle height is almost constant during the simulation, with null vertical velocity.

The last column on Figure 7.10 shows that for cavities with small width, the drag force over the particle increases and that is way the particle gets higher velocities and quickly moves upward. Observe also that the velocity vector changes its orientation during the simulation.

7.4

Single particle flotation

In this section we validate our floating particles formulation, observing the equilibrium position of one floating particle. The basic setup in the next examples is the following: the domain Ω is a closed box with dimensions $[-1.1, 1.1] \times [-0.5, 0.5]$ discretized by a mesh of 254 squared elements and filled with two Newtonian incompressible fluid phases Ω_{f_1} and Ω_{f_2} . The density and the viscosity of the upper and lower fluid phases are different in each example and will be defined later for each test case. One particle with radius $R_p = 0.14$ is embedded on the fluid and is initially at rest at the position $(0.0, -0.25)$.

Figure 7.11 shows the evolution and the final position obtained by three simulations using different densities for the particle. In this case the density of each fluid phase was $\rho_{f_1} = 1.0$ and $\rho_{f_2} = 0.0$ and their viscosity $\mu_{f_1} = 0.01$ and $\mu_{f_2} = 0.001$. From left to right, the particle's density ρ_p was 0.3, 0.5 and 0.8. In this example, the vertical component of the capillarity force was not considered.

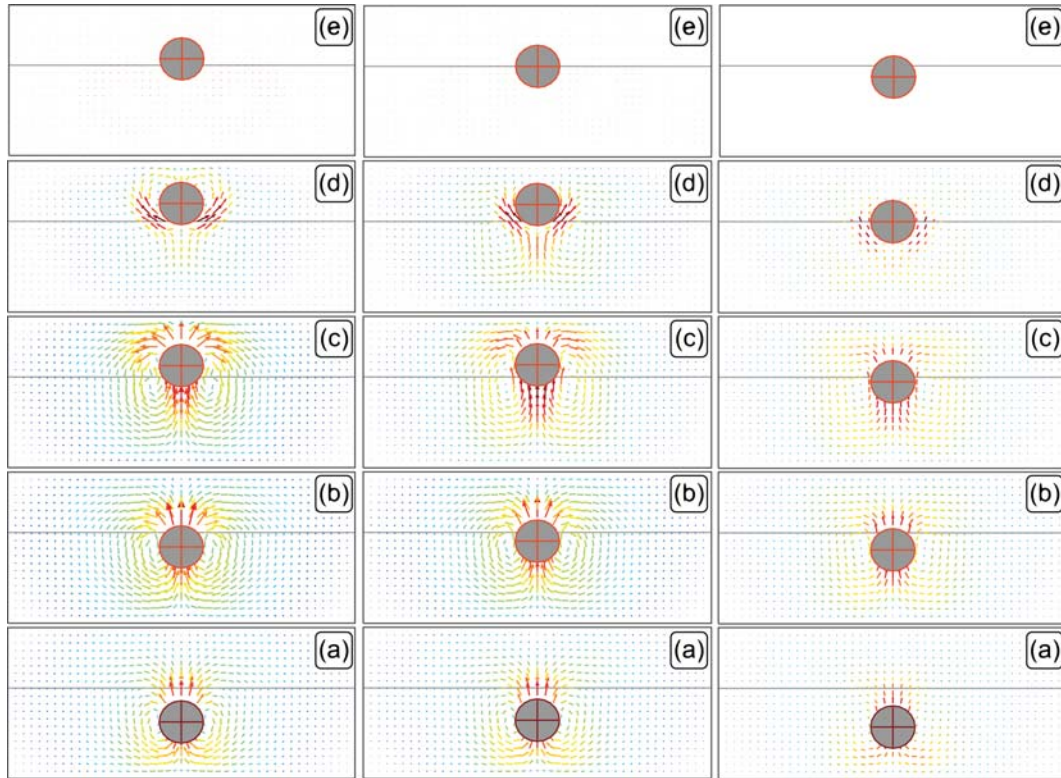


Figure 7.11: Single particle sedimentation: the equilibrium height of flotation varies when we change the particle's density. From left to right, its value was set to be $\rho_p = 0.3$, $\rho_p = 0.5$ and $\rho_p = 0.8$.

When $\rho_{f_2} = 0.0$, we can validate the buoyancy force computation verifying the immersed volume of the particle. In these cases, the immersed volume V_s must be equal to $V_s = \frac{\mu_p}{\mu_{f_1}} V_p$. So, if ρ_p were 0.3, 0.5 and 0.8 the theoretical immersed volumes V_s must be 0.3, 0.5 and 0.8. In our code, the immersed volumes obtained were 0.3117, 0.4864 and 0.8189 that represents an error of around 2% and shows that the equilibrium state obtained by our code agrees with the theory.

Figure 7.12 shows the velocity profile of the fluid phases at the vertical line that passes through $(0.0, -0.5)$ and $(0.0, 0.5)$ in each of the previous example (from left to right) at an instant of time equal to $0.3 ds$. The profile of the horizontal component is painted in blue, while the vertical component profile is shown in red. The interface between the two liquid phases is located at $y = 0.12$. At the interface between the phases, predicted discontinuity of the derivative of the profiles is related to the viscosity ratio of the two phases.

Figure 7.13 shows another test on single particle flotation. At this time, the particle's density and the lower fluid's physical properties are fixed and set to be $\rho_p = 0.5$, $\rho_{f_1} = 1.0$ and $\mu_{f_1} = 0.01$. The properties of the upper

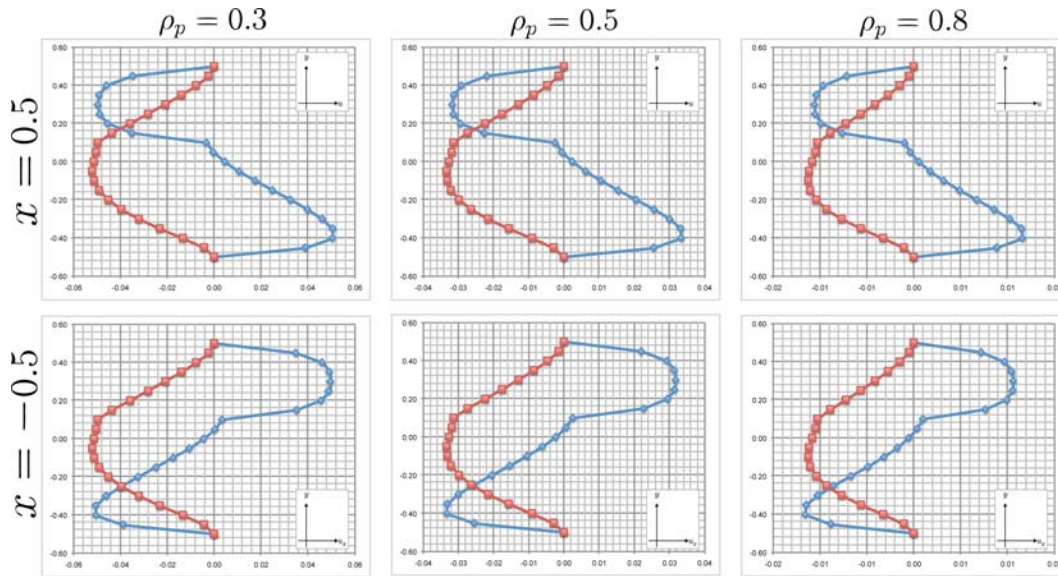


Figure 7.12: Single particle sedimentation: velocity profiles obtained from the simulations of Figure 7.11 (reading from left to right), measured on a vertical line that passes through $(0.0, -0.6)$ (see first row) and $(0.0, 0.6)$ (see second row). The blue lines are the profiles of the first and the red ones the profiles of the second coordinate functions of the velocity.

fluid phase varies, from left to right its density is $\rho_{f_2} = 1.0$, $\rho_{f_2} = 0.025$ and $\rho_{f_2} = 0.01$ and the viscosity is $\mu_{f_1} = 0.01$, $\mu_{f_1} = 0.0025$ and $\mu_{f_1} = 0.001$. Observe that as we decrease the top liquid density, the particle tends to be half immersed in the lower fluid and half inside the upper fluid at equilibrium, as expected.

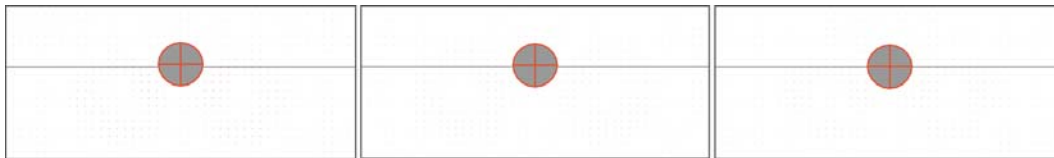


Figure 7.13: Single particle sedimentation: The flotation height varies when we change the fluid's properties. From left to right, the upper fluid's densities are set to 0.1, 0.025 and 0.01 and its viscosity 0.01, 0.0025 and 0.001.

Finally, Figure 7.14 shows the effect of the vertical component of the capillarity force when the fluid phases have densities $\rho_{f_1} = 1.0$ and $\rho_{f_2} = 0.1$ and viscosities $\mu_{f_1} = 0.01$ and $\mu_{f_2} = 0.001$. From left to right, the surface tension parameter on the capillarity computation was set to vary from 0.06 to 1.2. We observe that the final position of the particle changes as we increase the surface tension parameter.

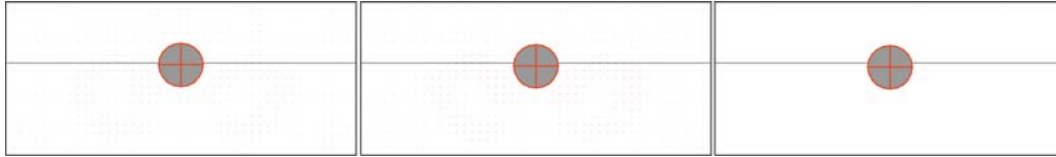


Figure 7.14: Single particle sedimentation: The equilibrium height of flotation varies when we change surface tension parameter when computing the capillarity force. From left to right its value is set to 0.06, 0.09 and 0.12.

7.5

Horizontal capillarity force

The last problem presented in this thesis aims to study the final arrangement of a set of particles floating at the interface between two fluid phases. As we said before on chapter 5, one of the physical phenomena that determine this final disposal is the horizontal component of the capillarity force, that occurs in particle–particle and particle–wall interactions. We show that, given different initial configurations for the same set of particles, their final arrangement may be completely different.

For all examples shown in this section, the basic set of parameters is the following: the domain Ω is a closed box with dimensions $[-1.0, 1.0] \times [-0.5, 0.5]$, discretized by a mesh of 253 squared elements with \mathbb{P}_4 – \mathbb{P}_2 finite elements basis functions. The fluid phase Ω_f is filled with two Newtonian incompressible fluid phases with interface height 0.7. The lower phase's density is defined to be $\rho_{f_1} = 1.0$ and its viscosity is $\mu_{f_1} = 0.01$ and the upper fluid parameters is set to $\rho_{f_2} = 0.0$ and its viscosity is $\mu_{f_2} = 0.01$. A single particle with radius $R_p = 0.14$ is embedded on the fluid. The particles are initially at rest in random positions that we describe later. The simulation's time step is $\delta t = 0.01$ deciseconds and the total simulated time is 10 seconds. Finally, we set the Lagrange multiplier parameter α to be 150.

Figure 7.15 shows two different simulations using almost the same initial configuration. A pair of particles with initial position, $\vec{X}_{p_1} = [-0.5, -0.15]$ and $\vec{X}_{p_2} = [0.5, -0.15]$ in the left column and $\vec{X}_{p_1} = [-0.25, -0.15]$ and $\vec{X}_{p_2} = [0.25, -0.15]$ in the right column, flow in the lower fluid until they float at the interface between the fluids. The left column shows five key frames of the simulation and as we see the particles are not near enough at the interface so there is no horizontal component of the capillarity force to attract each other. In the right column, the particles are closer and by capillarity the particles are attracted to each other when they reach the interface.

Figure 7.16 shows other two simulations. In the example on the left, we see the simulation of three particles, initially at rest inside the lower fluid. In

this example the first particle on the left is attracted to the wall due to the capillarity, while the other two particles are attracted to each other. In the right column, four particles initially at rest fall from the upper fluid phase and drop in the lower fluid phase. The particles float at the interface between the fluids, and don't attract each other. This happens because, in this example, the influence radius of the lateral capillarity is smaller than in the previous ones. The force is not strong enough to make the particles form clusters.

Finally, Figure 7.17 illustrates the simulation of the motion of five particles initially at rest on the upper fluid phase that fall down, drop in the lower fluid phase, float at the interface, forming clusters due to action of the horizontal capillarity force. The left column shows the particles falling and dropping in the lower fluid, while the left column details the clustering process. In this example the original set of particles creates two clusters one with four particles that are attracted to the left wall and the other with one particle attracted to the right wall. This example shows the potential of our method to a further study of the clustering formation problem, given a large set of particles.

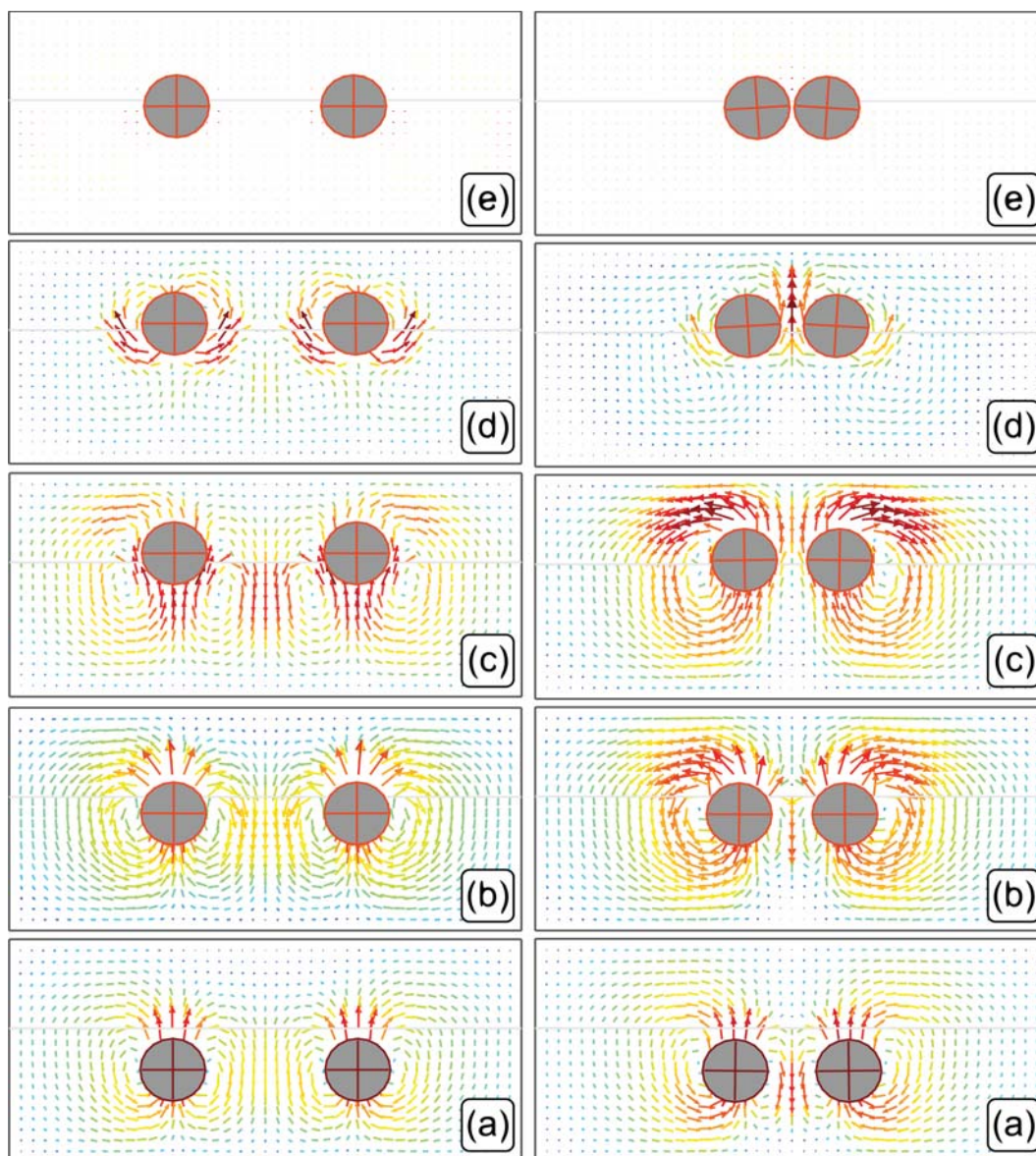


Figure 7.15: Two particles floating at the fluids interface: the particles are not near enough in the left column so the horizontal component of capillarity force doesn't exist and the particles are not attracted to each other. On the other hand, on the right column when the particles are close enough when they reach the interface they are attracted to each other.

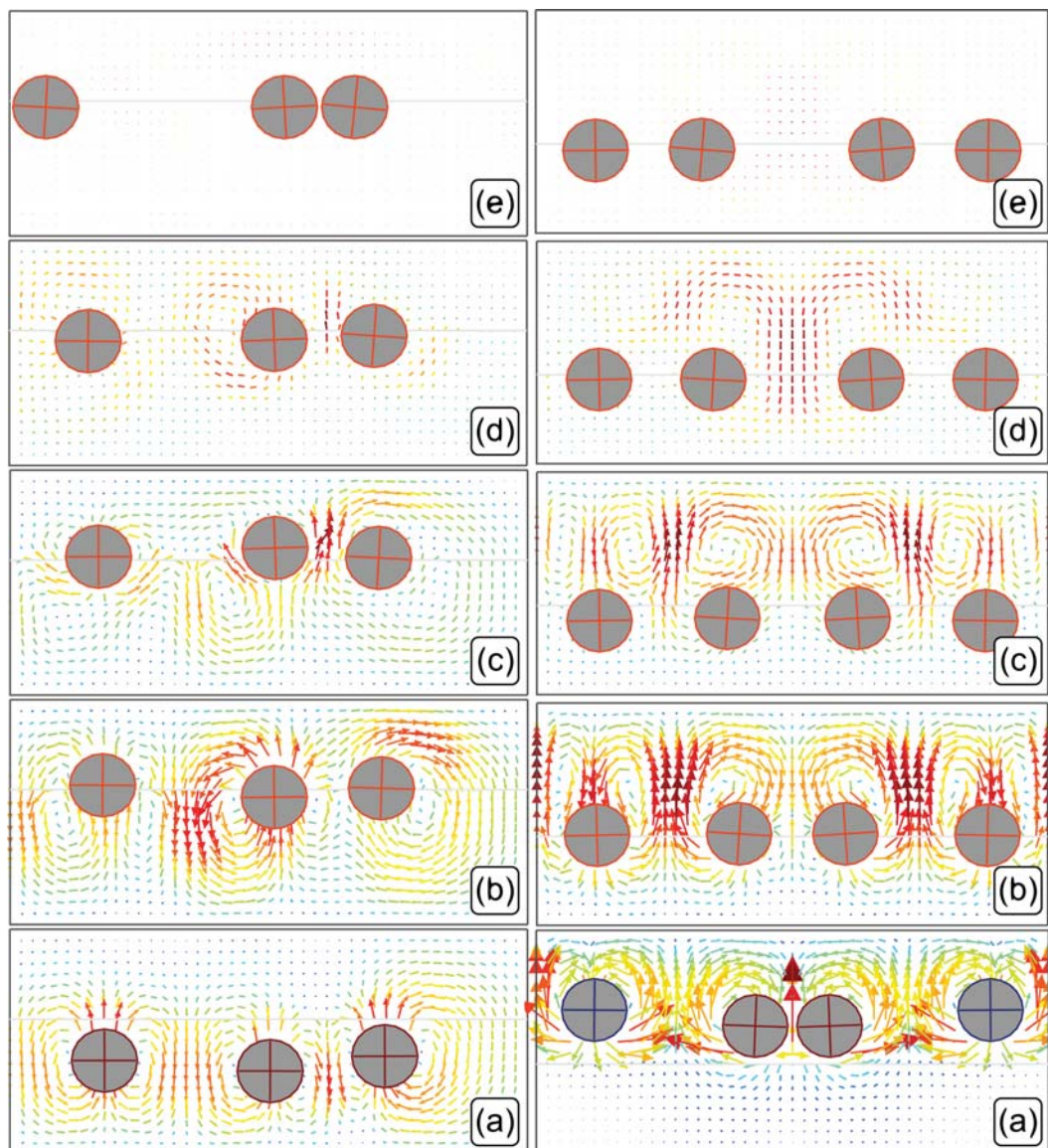


Figure 7.16: The left column shows the simulation of three particles, initially at rest on the lower fluid. Observe that the left particle is attracted to the wall while the two others attract each other. The right column shows four particles which are initially at rest, falling from the upper fluid phase and dropping in the lower fluid phase. As the influence radius of the capillarity force is small the particles don't form a cluster.

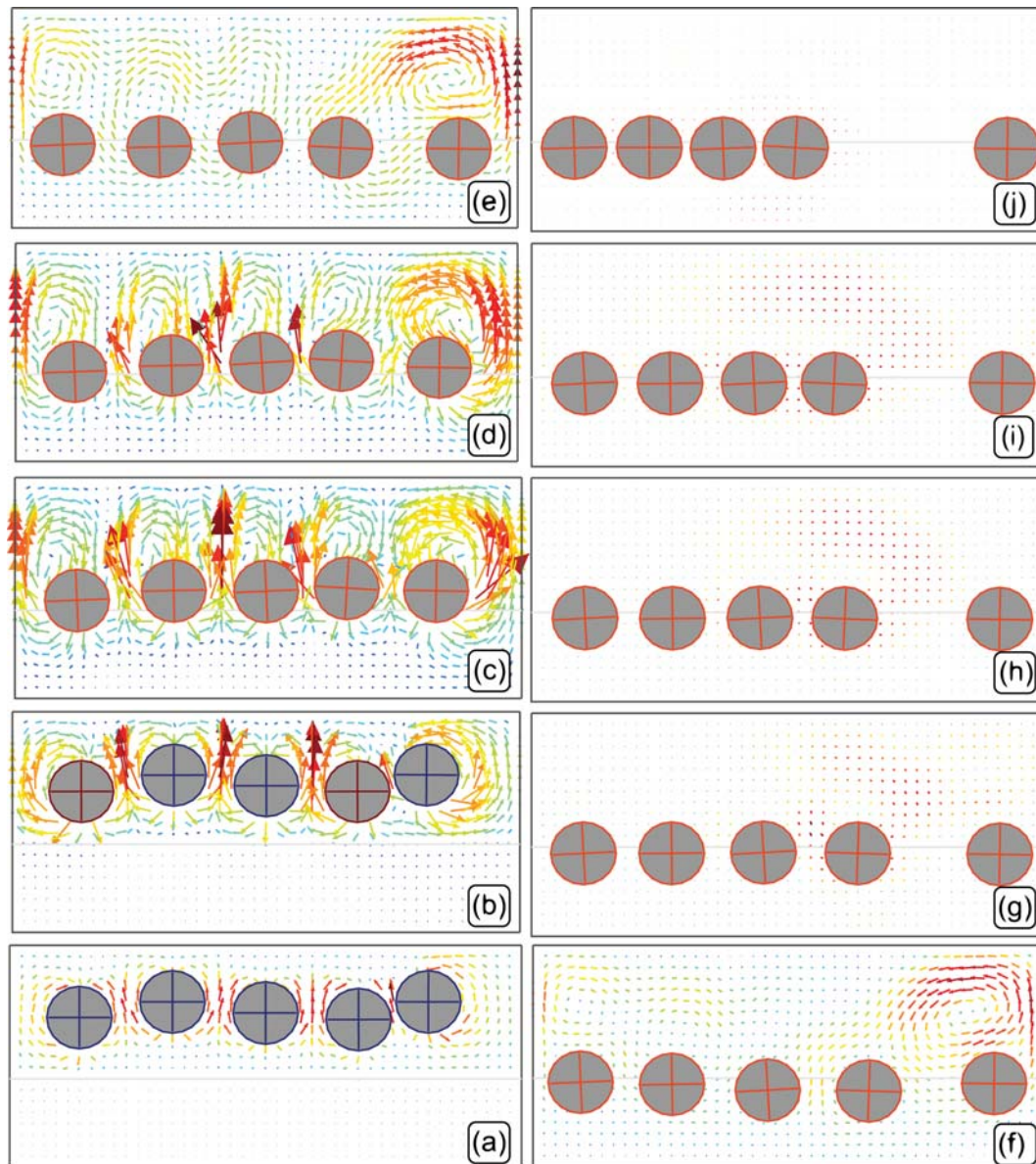


Figure 7.17: Floating particles clustering: five particles initially at rest on the upper fluid phase that are falling down, drop in the lower fluid phase (left column) and after floating at the two fluids interface, form two clusters near the walls due to action of the horizontal capillarity force (right column).